3D ACOUSTIC MAPPING OF THE KUROSHIO
(TAIWAN CURRENT) OFF THE SOUTHEAST COAST OF TAIWAN

Arata Kaneko, Professor
Graduate School of Engineering
Hiroshima University
1-4-1 Kagamiyama, Higashi-Hiroshima 739-8527, Japan
TEL/FAX: +81-082-424-7625
E-mail: akaneko@hiroshima-u.ac.jp

INTRODUCTION

Ocean acoustic tomography (OAT) is a powerful tool that can estimate the structure of sound speed (mainly proportional to temperature) and current in the ocean (Munk et al., 1995). Other than coastal sea studies (e.g., Park and Kaneko, 2000), most previous experiments have been carried out in the open ocean, characterized with a full structure of the underwater sound channel (Worcester, 1985; Cornuelle et al., 1985; Howe et al., 1987; Cornuelle et al., 1993; Dushaw et al., 1994; Send et al., 1995; Dushaw et al., 1995; Yuan et al., 1999). However its application to shallower regions with a sound speed profile (SSP) decreasing toward the bottom from the surface was limited because of the difficulty of ray resolvability (DeFerrari and Nguyen, 1986). The same reason leads to its infrequent application to the western boundary current regions, located along the continental slopes.

An OAT system, placed near the underwater sound channel axis where only its upper half is constructed, provides an efficient method to measure the full-depth profile of current in the Luzon Strait with the Kuroshio intrusion and strong internal tide activity, as demonstrated in the 2008 Luzon Strait experiment (Taniguchi et al., 2010).

In this study we apply the strategy employed by the 2008 Luzon Strait experiment to an analysis of acoustic tomographic data obtained in the Kuroshio southeast of Taiwan in 2009. The emphasis is on determining the time-dependent current profile above the sound channel axis that is near the bottom.

EXPERIMENT

An OAT experiment composed of two acoustic stations (T1 and T2) separated by about 47 km was carried out in the Kuroshio southeast of Taiwan from August 20 to September 15, 2009 (**Fig. 1**). The seafloor depth ranges from 900 m to 1300 m along the section between the tomographic stations. The precise distance between T1 and T2 (48.069 km) is estimated from the deployment GPS position of the subsurface moorings. The horizontal and vertical movement of the instrumentation on the short moorings was not measured because these movements have a small effect on the estimates of current velocities in this work. At each acoustic station, T1 and T2, an 800 Hz narrow-band organ pipe transducer with 50-Hz bandwidth (after series tuning; Engineering Acoustics Inc.) was attached at a

Report Documentation Page

1. REPORT DATE	2. REPORT TYPE	3. DATES COVERED
2012	**N/A**	**-**

4. TITLE AND SUBTITLE	5a. CONTRACT NUMBER
3D Acoustic Mapping Of The Kuroshio (Taiwan Current) Off The Southeast Coast Of Taiwan	5b. GRANT NUMBER
	5c. PROGRAM ELEMENT NUMBER

6. AUTHOR(S)	5d. PROJECT NUMBER
	5e. TASK NUMBER
	5f. WORK UNIT NUMBER

7. PERFORMING ORGANIZATION NAME(S) AND ADDRESS(ES)	8. PERFORMING ORGANIZATION REPORT NUMBER
Graduate School of Engineering Hiroshima University 1-4-1 Kagamiyama, Higashi-Hiroshima 739-8527, Japan	

9. SPONSORING/MONITORING AGENCY NAME(S) AND ADDRESS(ES)	10. SPONSOR/MONITOR'S ACRONYM(S)
	11. SPONSOR/MONITOR'S REPORT NUMBER(S)

12. DISTRIBUTION/AVAILABILITY STATEMENT
Approved for public release, distribution unlimited

13. SUPPLEMENTARY NOTES
The original document contains color images.

14. ABSTRACT

15. SUBJECT TERMS

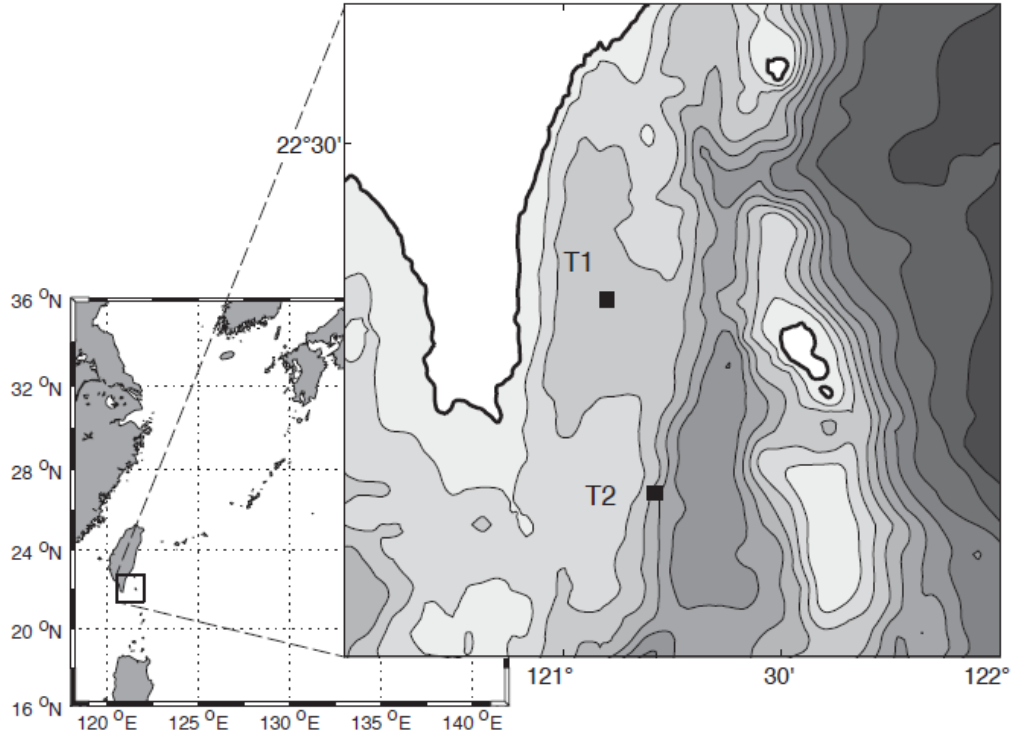| 16. SECURITY CLASSIFICATION OF:			17. LIMITATION OF ABSTRACT	18. NUMBER OF PAGES	19a. NAME OF RESPONSIBLE PERSON
a. REPORT	b. ABSTRACT	c. THIS PAGE	**SAR**	**14**	
unclassified	**unclassified**	**unclassified**			

FIG. 1 Location maps of the observation site. The bathymetric chart around the observation site is shown in a magnified scale in the right side of the figure (contour interval is 500 m). The square symbols indicate the locations of two mooring stations T1 and T2, each equipped with an OAT system. T1 was moored at 1243.5-m depth near 22° 10.343'N, 121° 5.877'E, and T2 was at 1330.3-m depth near 21° 45.049'N, 121° 12.542'E. Both OAT systems were suspended about 200 m above the seafloor.

depth of approximately 1,000 m to the mooring line, 200 m above the bottom. The source level of the transducer is about 13.2 W (182 dB re 1μPa at 1 m) and the electrical power consumption is 32 W, much smaller than that used in conventional, longer-range and lower frequency tomographic experiments. The transmitted signal consisted of a phase modulated linear maximal pseudorandom sequence, to achieve adequate signal-to-noise ratio and high time resolution. The parameters of acoustic signal are listed in **Table 1.** Sound was transmitted from both the subsurface systems every 1.5 hours, 10 minutes apart (not simultaneous due to the pulse length greater than the station-to-station distance as well as instrumentation constraints). Since our main focus is on measuring the Kuroshio Current, we apply a 5-day Hamming window to smooth the time series of differential travel times (described below), which suppresses noise including travel time variations caused by internal tides and waves.

Table 1. Transmission signal parameters

Carrier frequency, f_0	800 Hz
Order of M-sequence	12
Q, cycles per digit	12
Digit duration	15 ms
Sequence length	4095 digits
Period duration	61.425 s
Number of periods	1

The internal quartz oscillator drifted significantly during the experiment and could not produce accurate absolute differential travel times related to absolute currents. Therefore the clock correction method proposed by Worcester (1977) and Taniguchi et al. (2010) is applied here. In this study, typically differential travel times are small, less than 7 ms. Hence highly accurate clocks, such as an atomic oscillator, are desired for a subsurface OAT experiment where the system cannot receive GPS signals. However when applied to a subsurface moored system, the power requirements of a conventional atomic oscillator result in a large electrical power consumption with corresponding large and expensive battery packs (Worcester et al., 1985). A method for clock correction in which currents for the overlying layers are calculated relative to the deepest layer has already been used (Worcester et al., 1977; Taniguchi et al., 2010). As a result, the travel times for rays passing through the upper layers are referenced to near axial rays by this procedure. If current meter data are available in the deepest layer, the relative values of currents of the upper layers can be converted to the absolute values.

The shipboard ADCP (RDI 150 kHz Ocean Surveyor) was used to collect data along path T1-T2 three times on August 19. The ADCP measured the ocean currents between 10 m and 150 m below the sea surface. The raw ADCP velocities, acquired with a bin length of 8 m, were processed using a phase-averaging method to remove tidal variations (Chang et al., 2008) and compared with the OAT data. On the mooring line T1, a current meter was attached 10 m above the transceiver. CTD casts were conducted at the acoustic stations, T1 and T2, during the deployment and recovery cruises to provide estimates of the sound speed fields.

FORMULATION OF THE TOMOGRAPHY PROBLEM WITH CLOCK CORRECTION

The total travel time for the i-th acoustic ray path is composed of the contributions from path segments in N depth layers (counting from the deepest layer),

$$\tau_i^{\pm} = \sum_{j=1}^{N} \frac{l_{ij}}{C_j \pm u_j} \pm \tau_{\text{err}}, \quad i = 1, 2, \square, M \tag{1}$$

for a transmission in the positive/negative direction, respectively. C_j and u_j are the range-averaged sound speed and current for the j-th layer, respectively. The l_{ij} is the arc length traveled by the i-th ray in the j-th layer. The τ_{err} is the relative clock error for the paired station (the difference between the absolute clock errors at each station) and is a constant for all rays. Notice here $j = 1$ corresponds to the deepest layer. When calculating the differential travel time for the i-th ray, the clock error τ_{err} still appears, with a factor of 2, as shown below:

$$\Delta\tau_i \left(= \tau_i^+ - \tau_i^-\right) = \sum_{j=1}^{N} \left(-2\frac{l_{ij}u_j}{C_j} + 2\tau_{err} \right), \qquad i = 1, 2, \cdots, M. \tag{2}$$

It can be expressed in a matrix form as,

$$\begin{bmatrix} \Delta\tau_1 \\ \Delta\tau_2 \\ \vdots \\ \Delta\tau_M \end{bmatrix} = \begin{bmatrix} \dfrac{-2l_{11}}{C_1^2} & \dfrac{-2l_{12}}{C_2^2} & \cdots & \dfrac{-2l_{1N}}{C_N^2} \\ \dfrac{-2l_{21}}{C_1^2} & \dfrac{-2l_{22}}{C_2^2} & \cdots & \dfrac{-2l_{2N}}{C_N^2} \\ \vdots & \vdots & \ddots & \vdots \\ \dfrac{-2l_{M1}}{C_1^2} & \dfrac{-2l_{M2}}{C_2^2} & \cdots & \dfrac{-2l_{MN}}{C_N^2} \end{bmatrix} \begin{bmatrix} u_1 \\ u_2 \\ \vdots \\ u_N \end{bmatrix} + \begin{bmatrix} 2\tau_{err} \\ 2\tau_{err} \\ \vdots \\ 2\tau_{err} \end{bmatrix} \tag{3}$$

The τ_{err} can be eliminated by subtracting the differential travel time of a specific ray from those of all rays. Notice that the equation subtracted from itself becomes $0 = 0$, which is indefinite. If other independent information of current is available (i.e., current in specific layer), this information can be used to replace the indefinite equation. For example, if the first (deepest) ray is selected as a reference and some current information for the first layer (referred to as u_{ref}) is given, the differential travel times relative to the first ray ($\Delta\tau_{21}$, $\Delta\tau_{31}$,..., $\Delta\tau_{M1}$) may be expressed as:

$$\begin{bmatrix} u_{ref} \\ \Delta\tau_{21} \\ \vdots \\ \Delta\tau_{M1} \end{bmatrix} = \begin{bmatrix} 1 & 0 & \cdots & 0 \\ \dfrac{-2\left(l_{21}-l_{11}\right)}{C_1^2} & \dfrac{-2\left(l_{22}-l_{12}\right)}{C_2^2} & \cdots & \dfrac{-2\left(l_{2N}-l_{1N}\right)}{C_N^2} \\ \vdots & \vdots & \ddots & \vdots \\ \dfrac{-2\left(l_{M1}-l_{11}\right)}{C_1^2} & \dfrac{-2\left(l_{M2}-l_{12}\right)}{C_2^2} & \cdots & \dfrac{-2\left(l_{MN}-l_{1N}\right)}{C_N^2} \end{bmatrix} \begin{bmatrix} u_1 \\ u_2 \\ \vdots \\ u_N \end{bmatrix} \tag{4}$$

There are two ways to specify u_{ref}. The first is to set it to zero and then the currents of overlying layers are determined relative to the first layer. The other way is to use the current meter data (u_{CM}) as u_{ref}. In this case, the reconstructed overlying currents are absolute currents.

Equation (4) can be reduced to the form

$$\mathbf{y} = \mathbf{E}\mathbf{x} \qquad (5)$$

where $\mathbf{y}$ is the data vector, $\mathbf{E}$ the observation matrix and $\mathbf{x}$ the unknown variable model vector containing the layer currents.

Two methods are used to reconstruct the vertical profiles of overlying currents: the explicit solution and the inversion accompanied by regularization technique, both described below.

A. Explicit solution

The tomographic domain is divided into N depth layers, taking into consideration the result of ray simulations as shown in the next section. We define ray groups in the following way. The first ray group travels through only the first (deepest) depth layer, and the second ray group travels through both the first and second depth layers, and so on, resulting in the number of ray groups M equal to the number of depth layers N (in this case $M = N = 3$). In this evenly determined case, the observation matrix $\mathbf{E}$ becomes a lower triangular matrix and the explicit solution can be obtained directly in the following sequential form:

$$u_1 = u_{\mathrm{ref}} = \frac{C_1^2}{2l_{11}}\Delta\tau_{11}$$

$$u_2 = -\frac{C_2^2}{2l_{22}}\left\{\Delta\tau_{21} + \frac{2(l_{21}-l_{11})}{C_1^2}u_1\right\}$$

$$u_3 = -\frac{C_3^2}{2l_{33}}\left\{\Delta\tau_{31} + \frac{2(l_{31}-l_{11})}{C_1^2}u_1 + \frac{2l_{32}}{C_2^2}u_2\right\} \qquad (6)$$

$$\vdots$$

$$u_N = -\frac{C_N^2}{2l_{MN}}\left\{\Delta\tau_{M1} + \frac{2(l_{M1}-l_{11})}{C_1^2}u_1 + \frac{2l_{M2}}{C_2^2}u_2 + \cdots + \frac{2l_{MN-1}}{C_{N-1}^2}u_{N-1}\right\}$$

where u_{ref} is the reference velocity in the first depth layer and $l_{1j} = 0$ for the j values except $j = 1$.

B. Inversion with regularization

The inversion with regularization method overcomes certain limitations of the explicit method. Specifically, the explicit method requires that the number of ray groups equals the number of depth

layers and the solution is degraded due to the propagation of errors. For such cases the inversion method is preferable, yielding a smoother solution by regularization (Rajan et al., 1987).

The cost function J consists of the data misfit and smoothness measure of solution vector $\mathbf{x}$:

$$J = \mathbf{n}^T \mathbf{n} + \lambda \mathbf{x}^T \mathbf{L}^T \mathbf{L} \mathbf{x} \qquad (7)$$

where λ is a Lagrange multiplier and superscript T denotes the transpose of the matrix. $\mathbf{n} = \mathbf{y} - \mathbf{E}\mathbf{x}$ is the error vector. $\mathbf{L}$ is a second derivative operator. This smoothness measure penalizes solutions that are rough in a second derivative sense.

By minimizing J, the expected solution $\tilde{\mathbf{x}}$ is given by

$$\tilde{\mathbf{x}} = \left(\mathbf{E}^T \mathbf{E} + \lambda \mathbf{L}^T \mathbf{L} \right)^{-1} \mathbf{E}^T \mathbf{y}. \qquad (8)$$

The λ is so chosen that the residual defined by $\|\tilde{\mathbf{n}}\|^2 = \|\mathbf{y} - \mathbf{E}\tilde{\mathbf{x}}\|^2$ is less than a pre-determined value of 1 $(\mathrm{ms})^2$ (corresponding to 2.5 cm/s for a 50-km range).

For this inversion method, the error covariance matrix P (called the uncertainty) may be expressed by (Munk et al., 1995; Cornuelle et al., 1989)

$$\mathbf{P} = \left(\mathbf{E}^T \mathbf{E} + \lambda \mathbf{L}^T \mathbf{L} \right)^{-1} \mathbf{E}^T \langle \mathbf{n}\mathbf{n}^T \rangle \mathbf{E} \left(\mathbf{E}^T \mathbf{E} + \lambda \mathbf{L}^T \mathbf{L} \right)^{-1} \qquad (9)$$

RAY SIMULATION AND GROUPING

Range-dependent ray simulation is used to determine the observation matrix $\mathbf{E}$ in Eq. (5), using the HYCOM model data provided by the Naval Research Laboratory (Chassignet et al., 2009) for the reference sound speed field. **Figure 2** shows the simulated ray diagram and travel time distribution together with typical snapshots of measured arrival patterns during the experiment. The sound speed profile used in the ray simulation is shown in the left panel of **Fig. 2a**. The temperature and salinity data supplied from the HYCOM data are used to construct sound speed profiles for the ray simulation. Six equally spaced temporally average profiles from August 1 to September 31, 2009 are determined along the 48 km transmission line. The sound speed profiles estimated from the CTD casts (blue for T1 and green for T2) and the HYCOM data (black for T1 and red for T2) are in good agreement. The sound speed is slower at the north station (T1) than at the south station (T2), implying that water is cooler toward the north. The sound speed and its gradient determine the path length and travel time of rays between two stations. Rays that travel through the lower water layer experience weak refraction, have shorter path lengths, and arrive at the receiver first (**Fig. 2a**). Rays that travel through the middle and upper layers experience more bottom and surface reflections, and these are classified

conventionally into refracted-bottom reflected (RBR) and surface reflected-bottom reflected (SRBR) rays. The simulated travel times are plotted against the launch angles (**Fig. 2b**). The multiple observed peaks in the arrival patterns (**Figs. 2c** and **2d**) scatter around the simulated travel times.

Significant peaks are identified in the arrival patterns of T1 and T2 as those with SNRs greater than 12 dB. Ideally pairs of reciprocal arrival peaks for T1 and T2 are required for the calculation of differential travel times, and thus path-averaged currents, but in this case this is not possible because of the observed variability in the number, amplitude and travel times of the peaks. This variability is likely a combination of factors including non-simultaneity of transmissions, bottom interactions, and non-reciprocity due to current shear. Considering the distribution of ray paths from the surface to bottom, we shall here divide arrival peaks into three arrival groups and pairs of arrival peaks are searched for within each group. The 1st, 2nd and 3rd ray groups (equivalent to the 1st, 2nd and 3rd arrival groups, respectively) are selected to travel through only the lower layer (> 500 m), the lower to middle layer (> 250 m) and all three (lower to upper) layers, respectively. In the subsequent analysis, only the first arrival times are used as data of the first ray group. The 2nd ray group has relative travel times from 70 ms to 140 ms, measured from the first arrival time. The 3rd ray group has relative travel times 140 ms or greater from the first arrival time. The arrival peaks of T2 that make pairs with those for T1 are searched for within the time delay of 2 ms ± 15 ms for the 2nd arrival group and 7 ms ± 15 ms for the 3rd arrival group. The mean difference times of 2 ms and 7 ms are obtained using the HYCOM data between T1 and T2, and the ± 15 ms comes from one digit width of the M sequence.

Arrival patterns for the first three days are stacked upward as the time proceeds (**Fig. 3(a)**). The colored dots are put on the arrival peaks which satisfy the above condition for identifying the pair of significant arrival peaks; blue for the 1st arrival peak, and green for the 2nd arrival group and red for the 3rd arrival group. Both T1 and T2 data are compared in **Fig. 3(b)**. The reciprocity of arrival patterns is not satisfied in some places and the resulting peaks for T1 do not appear for T2. The differential travel times are determined by averaging all related data within individual arrival groups. The identification errors of arrival peaks due to non-simultaneity of transmissions, bottom interactions, and non-reciprocity are much reduced through the grouping and averaging processes. The results are furthermore smoothed with the 5-day Hamming window to reduce noise.
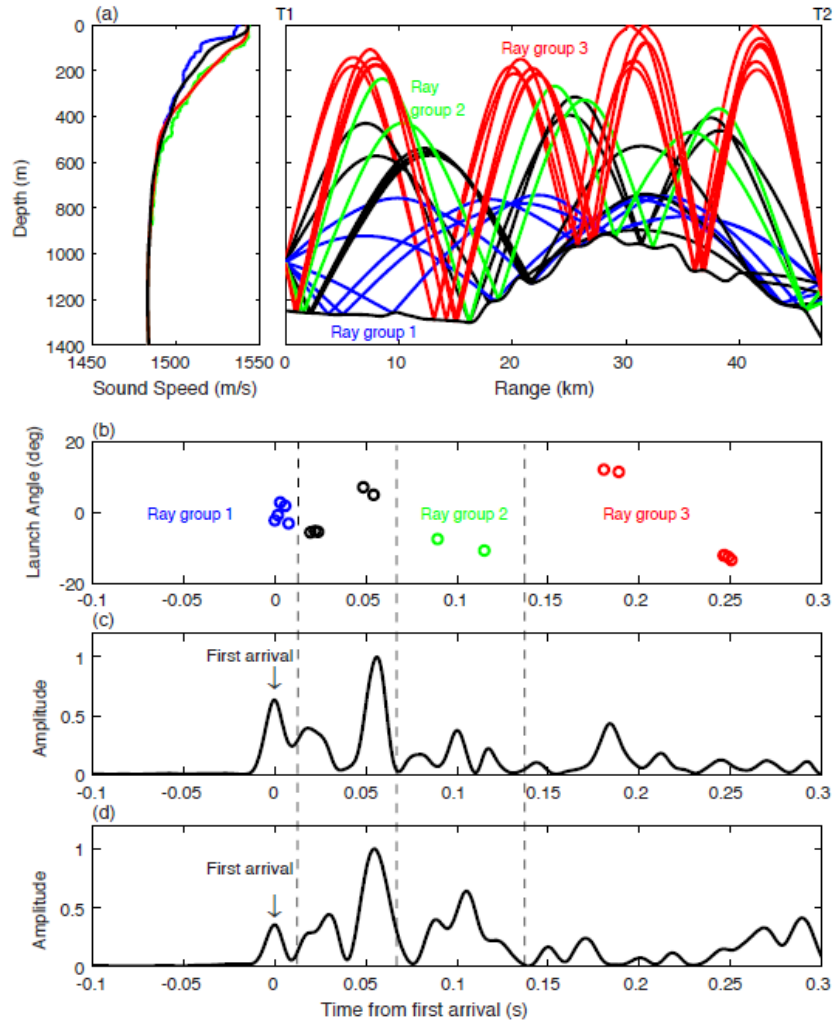
FIG. 2 Ray simulation and typical observed arrival patterns. Four sound speed profiles are shown in the left panel of (a): two are the temporal average of the HYCOM model and the other two are from CTD measurements, both are at T1 and T2, respectively. The results of the range-dependent ray simulation are shown with (a) the ray pattern and (b) the travel time - launch angle plot. Typical examples of the reciprocal arrival patterns observed at (c) T1 and (d) T2 are also shown. The green, blue and red colors are assigned for ray groups 1, 2, and 3, respectively. Individual ray groups are bounded with the dashed lines.
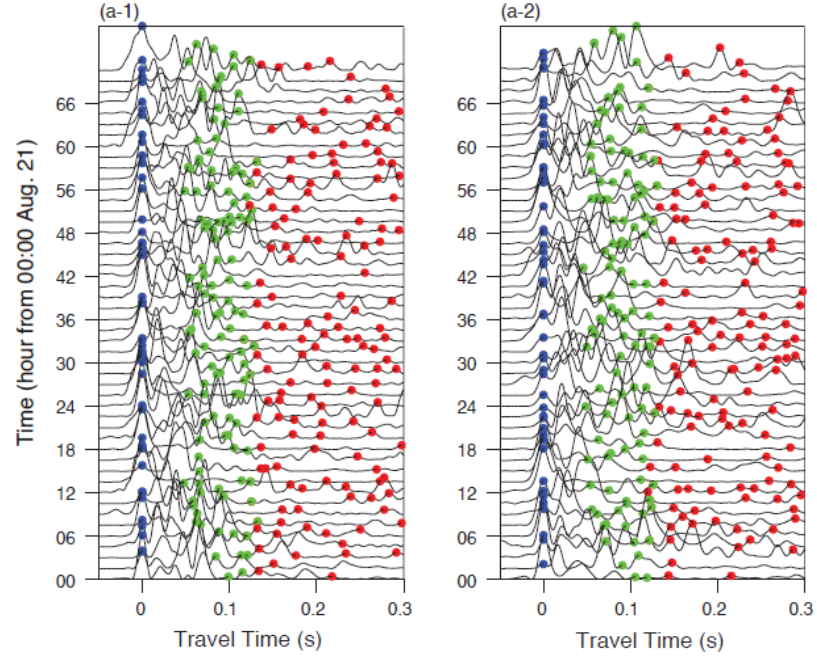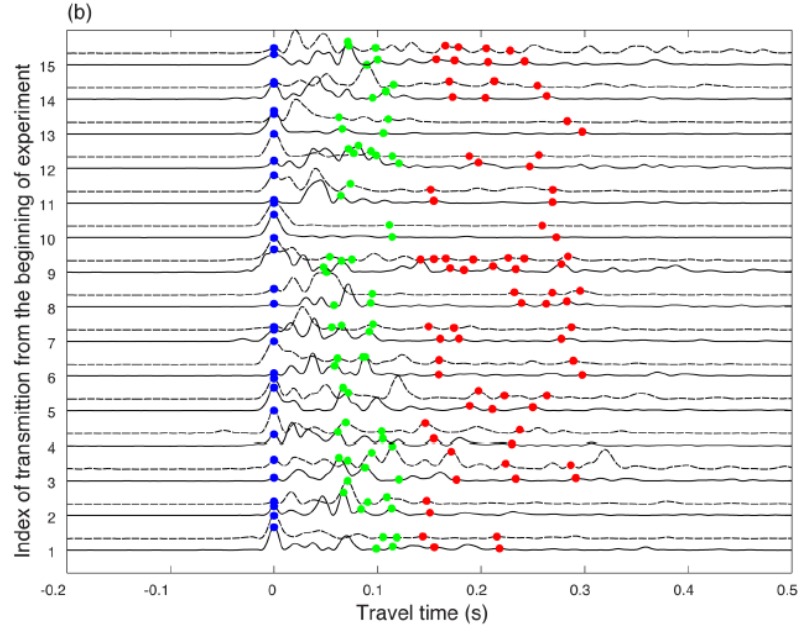
FIG. 3 (continue)

FIG. 3 Arrival patterns stacked upward with time. Data received at T1 and T2 are plotted separately in (a) for the first three days and together in (b) for the first day. In (b), solid lines are used for T1 and dashed lines for T2 with some offset from T1. The blue, green and red dots are put on the peaks that belong to ray groups 1, 2, and 3, respectively.

RESULTS

The currents in each layer determined from the explicit solution, Eq. (6), are shown in **Fig. 4** with the time series plotted together with the differential travel times for ray groups 2 and 3. Results for the two cases $u_{ref} = 0$ and $u_{ref} = u_{CM}$ are almost the same over the depth, because u_{ref} is small. The reconstructed current decreases from 0.4 m/s in the upper layer to 0.1 m/s in the middle layer. The lower layer current, obtained by the deep current meter, varies in the range from 2.2 cm/s to 3.6 cm/s. The upper and middle layer velocities are generally in-phase until September 10, but after that the in-phase relation is broken. Still, a 10-day oscillation is apparent over depth in spite of the limited observation period.

In the inversion, a six-layer model is used. Each layer has half the thickness of the layers in the explicit solution. Based on Eq. (8) and assuming $u_{ref} = u_{CM}$, the results are compared with the explicit solution in **Fig. 5**, after averaging two neighboring layers. The root mean square differences (RMSD) between the two solutions are 9.3 cm/s for the upper layer, 4.5 cm/s for the middle layer and 1.7 cm/s for the lower layer. The uncertainty determined from Eq. (9) is presented in the middle panel for the validity of inversion and the HYCOM currents are also shown in the lower panels for comparison. The inversion and the explicit solutions are very similar except that the vertical current shear is smaller for the inversion than for the explicit solution. The uncertainty (**Fig. 5(b)**) is smaller than 3 cm/s. The HYCOM data have a temporal variation similar to the current estimates.
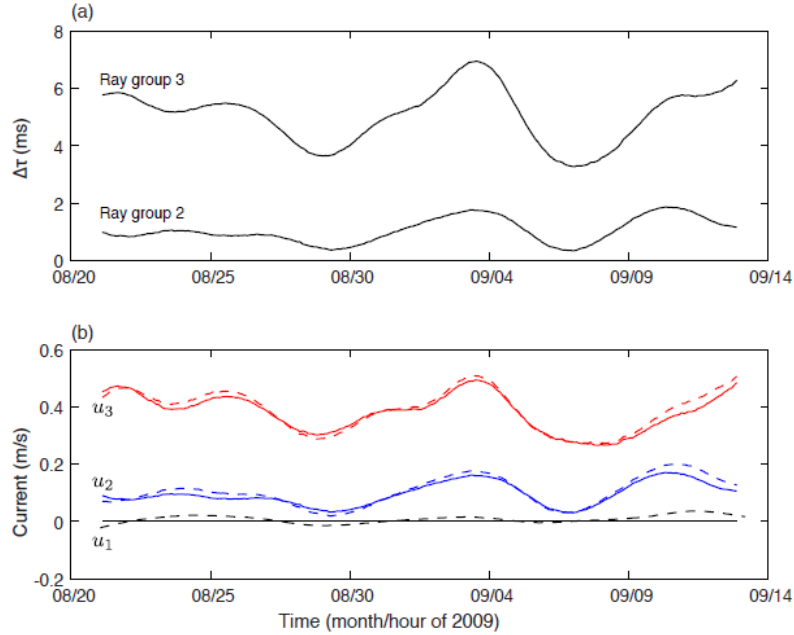

FIG. 4 Time series plots of (a) the differential travel times and (b) the reconstructed currents from the explicit solution (solid lines for $u_{ref} = 0$ and dashed lines for $u_{ref} = u_{CM}$).
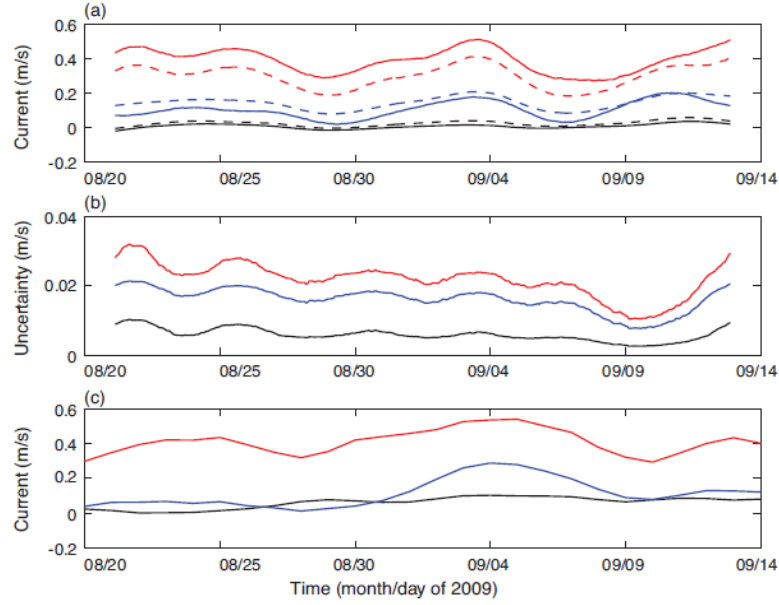
FIG. 5 (a) Comparison of the explicit solution (indicated by the solid lines) and inversion (the dashed lines). Both are obtained assuming $u_{ref} = u_{CM}$. (b) Uncertainty estimate for inversion with regularization. (c) HYCOM model data. The red, blue and black colors are assigned for the upper, middle and lower layers, respectively.

The vertical current profiles are constructed at depths of 125 m, 375 m, and 900 m that correspond to the midpoints of the respective layers (**Fig. 6**). The gradient of observed current is less for the inversion because of the smoothness constraint imposed in the regularization. The HYCOM data show the vertical profiles similar to the explicit solution, but the temporal variation of the HYCOM profiles is wider than that observed in the other solutions. The averaged shipboard ADCP profile taken on August 19 is compared with the explicit, inversion, and HYCOM profiles for August 21 (the center of 5-day smoothing window), in **Fig. 6 (d)**. A good agreement is obtained among the explicit solution, inversion and HYCOM data. The ADCP data differ from the other three measurements for the following possible reasons: 1) they are non-simultaneous measurements, with 2 day time difference, 2) the ADCP only covers the half of the upper layer, *i.e.,* 125 m, whereas the thickness of the layer is 250 m. If the ADCP data were extrapolated to 250 m depth, the agreement would appear better.

The temporal mean and standard deviation for all the current profiles are calculated for all the three layers and listed in **Table 2**. A good agreement of mean current is attained between the explicit solution and HYCOM data while the standard deviation for the HYCOM results in the middle layer is somewhat larger than for the other estimates.
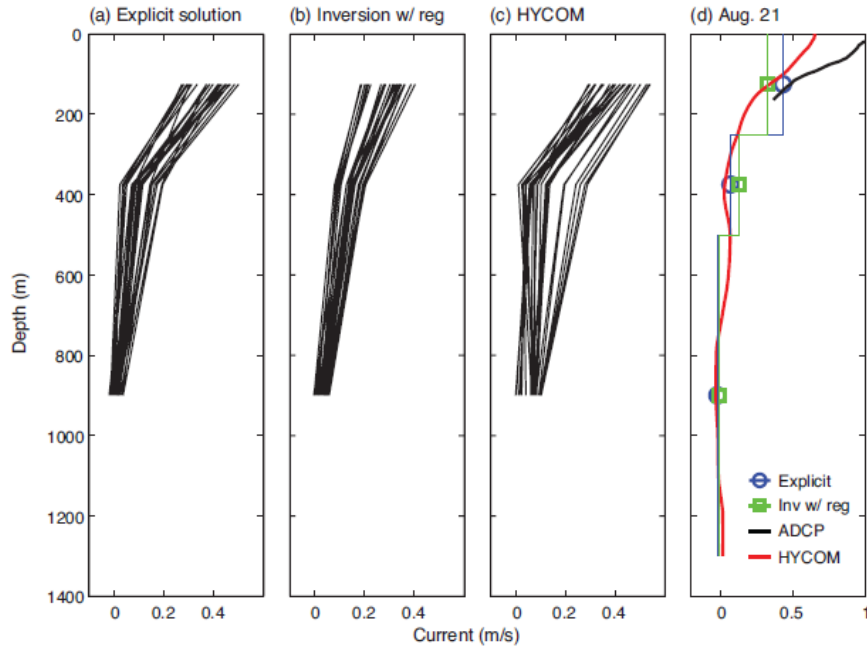
11

FIG. 6 Vertical profile of the depth averaged currents for (a) explicit solution, (b) inversion with regularization and (c) HYCOM data, obtained during the whole observation period. (d) The estimated profiles are compared with the measurement by the shipboard ADCP for the data on August 21.

Table 2. Comparing estimates of currents (temporal mean and standard deviation)

Layer	Depth-averaged current (cm/s)		
	Explicit solution	Inversion	HYCOM
Upper layer (0 - 250 m)	39 ± 7	30 ± 7	41 ± 7
Middle layer (250 - 500 m)	10 ± 5	14 ± 4	11 ± 8
Lower layer (500 - 1300 m)	0.8 ± 1.3	2.4 ± 1.7	6 ± 3

DISCUSSION

Range averaged vertical current profiles in the Kuroshio southeast of Taiwan were measured using two OAT transceiver systems, located 47-km apart near the underwater sound channel axis (at about 1,000 m depth). The reciprocal sound transmission data were successfully obtained at a repetition interval of 1.5 hours from August 20 to September 15, 2009. Because of a combination of factors (non-reciprocity due to bottom interaction and non-simultaneous transmissions, and low signal-to-noise ratio),

12

conventional procedures to pick the significant arrival peaks and make arrival-peak pairs for differential travel times were not applicable, so a new method of grouping and averaging for multiple arrival peaks has been developed and implemented here. Arrival peaks are divided into three ray groups. The differential travel times are determined as an average for each of three ray groups. The water column is also divided into three depth layers; the upper, middle and lower layers; the latter includes the underwater sound channel axis. The clock error is corrected for by setting the current of the lower layer either to zero or equating it to the deep current meter measurement that is small.

Two methods were used for reconstructing the vertical current profile. In the explicit solution, the number of ray groups equal the number of depth layers. The other solution is obtained by inversion with regularization, where the current at each depth is solved for simultaneously and the number of depth layers may be greater than the number of ray groups. Both results are in good agreement. Furthermore, the HYCOM model current and ADCP data along the sound transmission section are used for comparison with the tomographic data. The tomographic, model data and in situ measurements are in reasonable agreement.

The 10-day period oscillation is visible in all the three results (explicit solution, inversion and HYCOM), which is analogous to that observed in the East Taiwan Channel (Zhang et al., 2001) and may be caused by the baroclinic instability of the Kuroshio front east of Taiwan.

CONCLUDING REMARKS

Ocean acoustic tomography is a unique tool that can make long-term measurements of overlying currents from acoustic stations located near the underwater sound channel axis even if the vertical resolution is limited by the ray upper turning depth. The Kuroshio flowing above a continental slope is a natural application of the method because the deployed systems are compact, near the seafloor, and robust, in contrast to complicated and expensive point moorings that span the water column subject to trawling hazards and strong currents. Further, with now-available low power, accurate chip-scale atomic clocks, clock drift can be eliminated.

The successful use of ray groups to form differential travel times is basically an empirical result. It would be desirable to conduct acoustic numerical simulations that contain the effects of eddies, advection, internal waves, and bottom bathymetry to try and reproduce both the measured arrival patterns (taking into account the 10 minutes offset) and how they were sampled/processed to obtain the average group differential travel times.

REFERENCES

Cornuelle, B. D., C. Wunsch, D. Behringer, T. Birdsall, R. Heinmiller, M. Brown, R. Knox, K. Metzger, W. Munk, J. Spiesberger, D. Webb, R. Spindel, and P. Worcester (1985), "Tomography maps of the ocean mesoscale. Part 1: Pure acoustics," *J. Phys. Oceanogr.*, 15, 133-152.

Cornuelle, B., W. Munk, and P. Worcester (1989), "Ocean acoustic tomography from ships," *J. Geophys. Res.,* 94(C5), 6232-6250.

Cornuelle, B. D., P. F. Worcester, J. A. Hildebrand, W. S. Hodgkiss, T. F. Duda, J. Boyd, B. M. Howe, J. A. Mercer, and R. C. Spindel (1993), "Ocean Acoustic Tomography at 1000-km range using wavefronts measured with a large-aperture vertical array," *J. Geophys. Res.*, 98(C9), 16365-16377.

Chang, Y.-C., R.-S. Tseng, and C.-T. Liu (2008), "Evaluation of tidal removal method using phase average technique from ADCP surveys along the Peng-Hu channel in the Taiwan strait," *Terrestrial Atmospheric Oceanic Sciences*, 19(4), 433-443.

Chassignet, E.P., H.E. Hurlburt, E.J. Metzger, O.M. Smedstad, J.A. Cummings, G.R. Halliwell, R. Bleck, R. Baraille, A.J. Wallcraft, C. Lozano, H.L. Tolman, A. Srinivasan, S. Hankin, P. Cornillon, R. Weisberg, A. Barth, R. He, F. Werner, and J. Wilkin (2009), "US GODAE: Global ocean prediction with the HYbrid Coordinate Ocean Model (HYCOM)," *Oceanography,* 22(2), 64–75,

DeFerrari, H. A. and H. B. Nguyen (1986), "Acoustic reciprocal transmission experiments, Florida Straits," *J. Acoust. Soc. Am.,* 79(2), 299-315.

Dushaw, B. D. P. F. Worcester, B. D. Cornuelle, and B. M. Howe (1994), "Barotropic currents and vorticity in the central North Pacific Ocean during summer 1987 determined from long-range reciprocal acoustic transmissions," *J. Gephys. Res.*, 99, 3263-3272.

Dushaw, B. D., B. D. Cornuelle, P. F. Worcester, B. M. Howe, and D. S. Luther (1995), "Barotropic and Baroclinic Tides in the Central North Pacific Ocean Determined from Long-Range Reciprocal Acoustic Transmissions," *J. Phys. Oceanogr., 25*, 631-647.

Howe, B. M., P. F. Worcester, and R. C. Spindel (1987), "Ocean acoustic tomography: Mesoscale velocity," *J. Geophys. Res.*, 92(C4), 3785-3805.

Munk, W., P. F. Worcestor, and C. Wunsch (1995), *Ocean Acoustic Tomography*, Cambridge Univ. Press, Cambridge.

Park, J-H. and A. Kaneko (2000), "Assimilation of coastal acoustic tomography data into a barotropic ocean model," *Geophys. Res. Lett.*, 27(20), 3373-3376.

Rajan, S. D., J. F. Lynch, and G. V. Frisk (1987), "Perturbative inversion methods for obtaining bottom geoacoustic parameters in shallow sea," *J. Acoust. Soc. Am.*, 82(3), 998-1017.

Send, U., F. Schott, F. Gaillard, and Y. Desaubies (1995), "Observation of a deep convection regime with acoustic tomography," *J. Geophys. Res.,* 100, 6927-6941.

Taniguchi, N., A. Kaneko, Y. Yuan, N. Gohda, H. Chen, G. Liao, C. Yang, M. Minamidate, Y. Adityawarman, X. Zhu, and J. Lin (2010), "Long-term acoustic tomography measurement of ocean currents at the northern part of the Luzon Strait," *Geophys. Res. Lett.*, 37, L07601, doi:10.1029/2009GL042327.

Worcester, P. F. (1977), "Reciprocal acoustic transmission in a midocean environment," *J. Acoust. Soc. Am.*, 62 (4), 895–905.

Worcester, P. F., R. C. Spindel, and B. M. Howe (1985), "Reciprocal acoustic transmissions: Instrumentation for mesoscale monitoring of ocean currents," *IEEE J. Oceanic Eng.*, OE-10, 123-137.

Yuan, G., I. Nakano, H. Fujimori, T. Nakamura, T. Kamoshida, and A. Kaya (1999), "Tomographic measurements of the Kuroshio Extension meander and its associated eddies," *Geophys. Res. Letts*, 26(1), 79-82.

Zhang, D., T. N. Lee, W. E. Johns, C-T. Liu, and R. Zantopp (2001), "The Kuroshio east of Taiwan: Modes of variability and relationship to interior ocean mesoscale eddies," *J. Phys. Oceanogr.*, 31, 1054-1074.